Added mass and damping of an hexagonal rod vibrating in highly confined viscous fluids

Lucia Sargentini, Benjamin Cariteau

Added mass and damping of an hexagonal rod vibrating in highly confined viscous fluids

Lucia Sargentini* **and Benjamin Cariteau**
Université Paris-Saclay, CEA-Saclay,
Service de Thermohydraulique et de Mécanique des Fluides, 91191, Gif-sur-Yvette, France
lucia.sargentini@cea.fr

This paper deals with fluid-structure interaction analysis of an hexagonal rod enclosed in a narrow viscous gap.

A new analytical solution for a 2D cylindrical case is derived and described. A numerical solution of 2D Navier-Stokes equations coupled with an harmonic structure model is applied to both cylindrical and prism geometries. The comparison between the numerical tool and the analytical solution is discussed and a method to apply the analytical solution to the hexagonal case is proposed.

An original definition of the added mass and damping based on an energetic approach is provided avoiding the dependence from the geometry and the type of forcing (free or forced vibration).

An experimental facility is provided accounting for an hexagonal prism vibrating within a 7 mm enclosure. Free vibration experiments in water allow assessing the added mass and added damping effect on the modal parameters.

The fluid flow is affected by a 3D effect – named downstrokes flow – at the top and the base of the assembly because of free surface and stoky geometry. This produces a higher frequency than the 2D theoretical value given both by the analytical solution and the numerical simulation. A geometry-based correction factor is suggested to taken into account in the 2D numerical simulation the 3D effect.

Velocity measured within the gap provides further insight on this phenomenon and agrees well with the prediction of the transposed cylindrical analytical model.

Nomenclature

a Instantaneous amplitude [m].
a_0 Initial amplitude of free decay [m].
$\dot{a}$ Instantaneous solid velocity [m/s].
b Gap thickness [m].
C_a Added damping [kg/s].
C_D Added damping coefficient [–].
C_M Added mass coefficient [–].
$D_{i,j}$ Momentum diffusion [1/s].
$E_{c,f}$ Fluid kinetic energy [J].
E_{dis} Fluid dissipated energy [J].
$E_{t,s}$ Total solid energy [J].
E_0 Initial potential energy [J].
H Height of the prism [m].
M_{add} Added mass [kg].
R_1 Internal cylinder radius [m].
R_2 External cylinder radius [m].
Re Reynolds number Ub/ν [–].
St Strouhal number $\omega R_1/U$ [–].
U Tangential velocity scale [m/s].
V Radial velocity scale [m/s].
x Developed tangential coordinate [m].
y Developed radial coordinate [m].
r Radial coordinate [m].
t Time [s].
p Pressure [Pa].
δp Pressure variation scale [Pa].

Greek

β 3D-to-2D correction factor [–].
η Confinement ratio [–].
ρ Fluid density [kg/m^3].
ν Fluid kinematic viscosity [m^2/s].
ε Amplitude-to-gap ratio [–].
σ Stokes number $\omega b^2/\nu$ [–].
ω Angular frequency [s^{-1}].
χ Mulchay slenderness parameter [–].
θ Azimuthal coordinate [rad].
τ Time integration length [s].

1 Introduction

In Sodium Fast Breeder Reactor (Na-FBR) fuel assemblies are hexagonal prisms in a periodic lattice and, because of neutronic optimisation, they are arranged in a very narrow gap configuration. During vibrations, such confined configuration gives rise to high fluid forces acting on the hexagonal prisms, involving a modification on the structure's dynamic behaviour.

While in scientific literature fluid-structure interaction for cylindrical structures are largely discussed (see for in-

*Address all correspondence to this author.

stance the book of Païdoussis [1]), to the authors' knowledge only few works are specifically devoted to other geometries.

Recently, Zhong et al. [2] [3] perform some experiments to improve the comprehension of the fluid-structure interaction dynamic of the double graphite bricks in molten salt reactor. They find that finite element 2D analysis well represents the FSI experiments if bricks are sufficiently immerged in the water.

Daogang et al. [4] present some free vibration tests of two neighboring hexagonal prisms. Added mass and damping coefficients are evaluated experimentally showing a large dependence on the thickness of the fluid gap. It is suggested that Wilson's laws [5] are in good agreement with their experience. Nevertheless, no comparison is given. Moreover, Wilson's work shows a discrepancy between the given definition of the added mass coefficient and the experiences of Yang and Moran [6].

In his classical study, Fujita [7] performs a seismic response analysis of a group of 7, 19 or 37 hexagonal columns immersed in water. He proposes a two-dimensional semi-theoretical method based on the resolution of Euler equations coupled with mass-spring model for structure. The vertical flow of liquid is neglected and each assembly is supposed to vibrate parallel to its generating line. He suggests a value of the added mass for two concentric hexagonal rods with narrow gap showing a poor agreement with the experiences.

To study analytically a much simpler geometry, several authors investigate forced vibration of a two-dimensional cylindrical rod immersed in a fluid confined within a shell [8–10].

Mulcahy [11] proposes an extension of the 2D analytical solution of Chen [9, 12] to 3 dimensions for a finite length cylinder. Unfortunately, its solution is valid only far from the ends. Actually, the postulated fluid flow is two-dimensional with a vertical component of the velocity. Nevertheless, he presents a correlation between the fluid damping force and the geometrical aspect ratio of the finite cylindrical rod. We detail it later on the article.

In a previous communication [13], we presented an original analytical solution for the vibration of a two-dimensional cylindrical rod immersed in a fluid confined within a shell. We validated against it a coupled fluid-structure numerical solver that we used to investigate the flow differences between hexagonal and circular annulus. A transposition method was formulated to apply the cylindrical analytical solution to hexagonal prisms.

In this communication, we challenge the analytical solution against experimental data of added mass and fluid flow in the gap. In the next section we recall an analytical solution for the forced vibration of a long cylinder enclosed in a small viscous gap. Subsequently, the application to hexagonal prisms is discussed together with some three-dimensional fluid phenomena affecting short cylinders and prisms. Finally, we present some experimental results and we compare them to our analytical model.

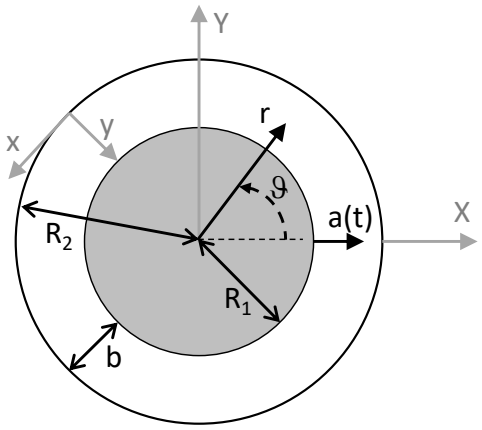

Fig. 1. Sketch of the cross-section of a cylinder vibrating in a thin fluid annulus.

2 Analytical solution for a cylinder vibrating in a small viscous gap and extension to hexagonal prisms

An original analytical solution is obtained for the forced vibration of a cylinder in a very confined viscous fluid with initially stagnant fluid. It was presented in a previous communication [13]. We resume here the main features and we give in appendix the (previously unpublished) explicit expression. Subsequently, by means of an available transposition criterion, it is applied to hexagonal geometries in Section 3.

Since the fluid is stagnant at the beginning of the movement, turbulent flow regime should not be able to develop for times as short as ≈ 0.1 s. If gap fluid is water or liquid sodium, the time scale which is necessary for the development of a boundary layer is much large than 0.1 s. Nevertheless, even if viscous effects seem to be negligible a priori, we consider important to gather a solution for validation of numerical models accounting for viscosity. In fact, viscosity plays a role for the vibration of hexagonal prisms [16].

The 2D Navier-Stokes equations are solved for an incompressible and viscous fluid flow in a very thin gap for forced bi-dimensional vibrations. A sketch of the studied configuration is shown in Fig. 1.

The external cylinder of radius R_2 is fixed while the internal cylinder of radius R_1 vibrates with amplitude $a(t)$. No-slip boundary conditions are used for the external and internal cylinder walls. Because of narrow gap hypothesis, the fluid domain can be assimilated to a developed cylinder area. Therefore a coordinate transform is applied, where $x = R_2\theta$ and $y = R_2 - r$.

A non-dimensional analysis may be performed finding all the unknown scales [15]. Let's define overlined quantities as non-dimensional parameters. U and V are the scale respectively of tangential $\bar{u}(\bar{x},\bar{y},\bar{t})$ and radial $\bar{v}(\bar{x},\bar{y},\bar{t})$ velocity. These velocity scales are unknown at the beginning of the analysis, as well as δp as pressure scale. Other scales are provided: the angular frequency ω is taken as time scale, the clearance of the gap b as y-scale, the external radius R_2 as

x-scale and the maximum of displacement a_0 as the scale of oscillation amplitude.

The following non-dimensional parameters are obtained from the equations :

- $\eta = b/R_2 \ll 1$ which represents the effect of confinement;
- $\varepsilon = a_0/b$ which represents the maximum amplitude of oscillation relating to the gap. This value is limited to 1 and can be very low;
- $\mathrm{St} = \omega R_1/U = 1/\varepsilon$ which is the Strouhal number. It represents the ratio between the displacement time of a fluid particle and the displacement time of the solid body. From boundary conditions we can see that the Strouhal number depends only on the geometry and on the amplitude of vibrations;
- $\mathrm{Re} = Ub/\nu$ which is the Reynolds number. As the fluid velocity scale is imposed by the vibration, Reynolds number contains frequency information ;
- $\sigma = \omega b^2/\nu$ which is the Stokes number.

The resulting velocity scales are :

$$\begin{cases} U = \varepsilon R_1 \omega \\ V = \eta U \end{cases} \tag{1}$$

The complete description of the velocity and pressure scales is available in Sargentini et al. [15]. The dimensionless Navier-Stokes equations finally become :

$$\begin{cases} \dfrac{\partial \bar{u}}{\partial \bar{x}} + \dfrac{\partial \bar{v}}{\partial \bar{y}} = 0 \\ \dfrac{\partial \bar{p}}{\partial \bar{y}} = 0 \\ \mathrm{St}_1 \dfrac{\partial \bar{u}}{\partial \bar{t}} + \left(\bar{v} \dfrac{\partial \bar{u}}{\partial \bar{y}} + \bar{u} \dfrac{\partial \bar{u}}{\partial \bar{x}} \right) = -\dfrac{\delta p}{\rho U^2} \dfrac{\partial \bar{p}}{\partial \bar{x}} + \dfrac{1}{\eta \mathrm{Re}} \dfrac{\partial^2 \bar{u}}{\partial \bar{y}^2} \\ \bar{v}\big|_{\bar{y}=0} = 0 \qquad \forall \bar{x}, \bar{t} \\ \bar{u}\big|_{\bar{y}=0} = 0 \qquad \forall \bar{x}, \bar{t} \\ \bar{v}\big|_{\bar{y}=1} = -\cos(\bar{x}) \qquad \forall \bar{x}, \bar{t} \\ \bar{u}\big|_{\bar{y}=1} = 0 \qquad \forall \bar{x}, \bar{t} \\ \bar{v}\big|_{\bar{t}=0} = 1 \qquad \forall \bar{x}, \bar{y} \end{cases} \tag{2}$$

The azimuthal pressure gradient is the driving term of the fluid displacement. Therefore we deduce the pressure scale (i. e. Euler number) from the other scales :

$$\frac{\delta p}{\rho U^2} = \sup\left\{ \mathrm{St}; 1; \frac{1}{\sigma \varepsilon} \right\} \tag{3}$$

where the first group is the scale of non-stationary term, the second one is the scale of convective term and the last one is the scale of viscous term.

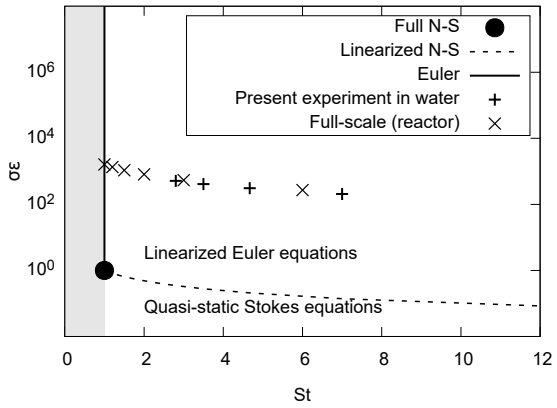

Fig. 2. Flow map for a solid rod vibrating in a thin fluid annulus.

From this system of equations, a flow regime map may be deduced which reveals the suitable mathematical model according to the physical condition to be described (Fig. 2). Strictly speaking, full Navier-Stokes (N-S) model is only required when $\mathrm{St} \sim \sigma\varepsilon \sim 1$.

When σ is lower than 1, viscous effects must be taken into account and quasi-static Stokes equations apply; when σ is higher, Euler equations apply. Moreover for small amplitude oscillation ($\varepsilon \gg 1$) linearized Euler equations apply. Full form of Navier-Stokes equations would be necessary when all scales equal.

The explicit solution of the equations 2 is given in appendix. Also, a solution for free decay vibration was obtained and detailed in reference [15]. Our solution is valide for very thin gap and, in these cases, it is in good agreement with the one provided by Chen [9]. With respect to Chen formulation, the present one allows easier numerical calculation (because of the absence of Bessel functions) and hence easier acces to the flow field (equation 9-10-11).

3 Extension of the cylindrical analytical solution to the hexagonal prism

Sargentini et al. [13] set up a 2D numerical tool which solves the full Navier-Stokes equation coupled to structure dynamics by means of Arbitrary Lagrangian-Eulerian mesh displacement (ALE) with the code Cast3M. A comparison between the free response of an enclosed cylinder and an hexagonal prism was studied. It was found that the 2D cylindrical analytical solution may be used to evaluate the fluid forces and flow for the hexagonal prism at middle-height. The only condition to satisfy is to set up a cylindrical analytical calculation having the same fluid cross section of the hexagonal case.

Using an energetic approach, we can give the following definitions for added mass and added damping:

- the added mass is the mass of the coupled system (liquid and solid body) which moves at the velocity of the solid

body. Hence the added mass coefficient C_M is:

$$C_M = \frac{1}{\rho \pi R_1^2} \frac{\int_0^\tau E_{c,f} dt}{\int_0^\tau \frac{\dot{d}^2(t)}{2} dt} \tag{4}$$

with τ as the time integration length and $E_{c,f}$ the fluid kinetic energy.

- the added damping is related to the energy E_{dis} dissipated by the coupled system. Let's define E_{dis} as :

$$E_{dis} = \int_0^\tau C_a(t) \dot{d}^2(t) dt \tag{5}$$

with $C_a(t)$ the instantaneous added damping. This dissipation occurs in the fluid, operated by the viscous forces. In other words:

$$E_{dis} = \int_0^t \int_\Omega 2 \frac{\nu}{\rho} \sum_{ij} \frac{\partial u_i(t)}{\partial x_j} D_{ij}(t) \, dA \, dt \quad \text{for } i, j = x, y$$

where $D_{ij} = \frac{1}{2} \left(\frac{\partial u(t)}{\partial y} + \frac{\partial v(t)}{\partial x} \right)$. The instantaneous dissipated energy $E_{dis}(t)$ can also be calculated as:

$$E_{dis}(t) = E_0 + E_{c,f}(t) + E_{ts}(t)$$

where E_0 is the initial energy of the system (i.e. the potential energy before the free vibration) and E_{ts} is the structure total energy (i.e. kinetic and potential energy). The average added damping coefficient C_D at instant τ can be estimated as:

$$C_D(\tau) = \frac{\tau}{\rho_f \pi R_1^2} \frac{E_{dis}(\tau)}{\int_0^\tau \dot{d}^2(t) \, dt} \tag{6}$$

Both the added mass and damping coefficients take the form of a power divided by an energy and are made dimensionless by using a mass. The added mass coefficient C_M is an average value during the time oscillation. On the contrary, the C_D depends on the time of the oscillation τ, since the damping coefficient can vary with the amplitude during vibrations.

Rather than Chen's dynamic formulation [9], our definitions are independent on the geometry of the system and the form of vibration. Recently, some works on two-phase flow added mass also turn towards an energetic approach [18].

For the cylindrical geometry, our definition and the analytical solution of Chen are in perfect agreement (Fig. 3 and Fig. 4). For the hexagonal geometry, validation is provided in Sargentini [15] through a comparison with the theory of Chung and Chen [14].

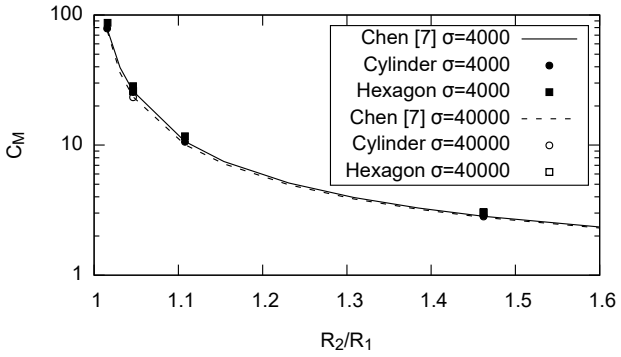

Fig. 3. Comparison between the calculated added mass coefficient for cylindrical and hexagonal geometry for different Stokes numbers σ as a function of the confinement.

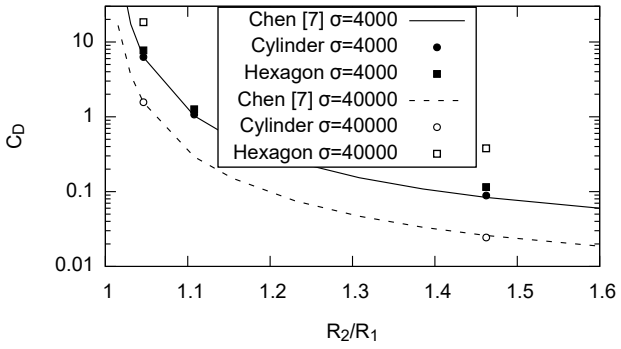

Fig. 4. Comparison between the calculatef added damping coefficient for cylindrical and hexagonal geometry for different Stokes numbers σ as a function of the confinement.

Results for the C_M for the two geometries are close, but the hexagonal solution is always slightly higher than cylindrical one. For C_D, the higher the frequency and thinner the gap, the more the difference between cylinder and hexagonal body. This discrepancy is due to the difference on the fluid velocity profiles, thus on the fluid kinetic energy, between cylindrical and hexagonal case. In fact, as the hexagon vibrates perpendicularly to one of its sides, the cylindrical analytical solution of tangential velocity describes well the fluid flow close to the mid-side of the prism. Conversely, the cylindrical analytical solution fails to estimate the flow close to the vertex of the hexagonal gap [15]. In Fig. 5, the 2D numerical results for the tangential velocity u in both cylindrical and hexagonal geometries is presented. The direction of vibration of the inner prism is $\theta = 0^\circ$ which, for the hexagonal case, is normal to the side. The cross-gap velocity profile is the same for both geometries for $\theta = 0^\circ$ (mid-side of the hexagon). On the contrary, the cross-gap velocity profile at the corner of the hexagon is different. In fact, the presence of these corners gives rise to recirculations (vortex) even in non-turbulent flows.

These vortices on the corners of the hexagon dissipate

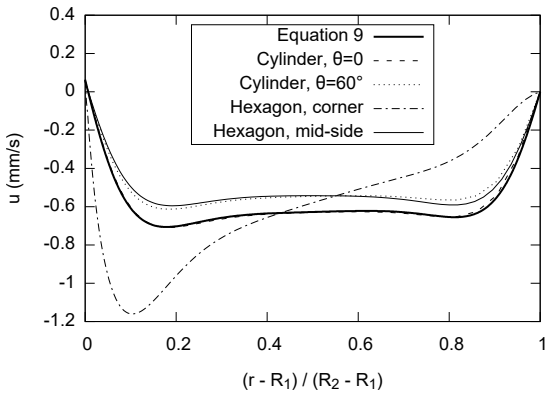

Fig. 5. Numerical results for the tangential velocity u in both cylindrical and hexagonal geometries [13]. Comparison is given with the analytical solution of system 2 given in appendix (equation 9).

Table 1. Dynamical characteristics measured on the twin blades-supported hexagonal prism enclosed in a 7 mm gap.

Frequency in air (Hz)	11.7
Damping ratio in air (%)	3.7
Frequency in water (Hz)	5.2
Damping ratio in water (%)	2.4
Added mass coefficient	5.5

energy and increase the added damping with respect to cylindrical geometry, thus explaining the discrepancies between the two geometries shown in Fig. 4.

4 Experimental results: comparison with theory

4.1 Experimental apparatus

The analytical study was used to design a test rig accounting for a single Poly-methyl methacrylate (PMMA) hexagonal prism enclosed in a 7 mm gap filled with water and named PISE-1a [13]. The prism is 71,4 mm of side and 500 mm tall.A picture is provided in Fig. 6.

The prism is free on top and supported by a twin blades system on the bottom. Blades are stainless-steel made, 3 mm thick and 210mm in height. This system allows solid-body, one-degree-of-freedom vibration of the prism, i.e. horizontal translation orthogonal to the generating lines. Strain gauges are fixed on the blades to recover prism displacement. Time-domain modal analysis is applied on displacement time-history to estimate the modal parameters [15].

Velocity fields within the gap are recorded by Particle Image Velocimetry (PIV) at a frequency of 500 Hz.

Free vibration response of the assembly are detailed in section 4.2 and Tab. 1.

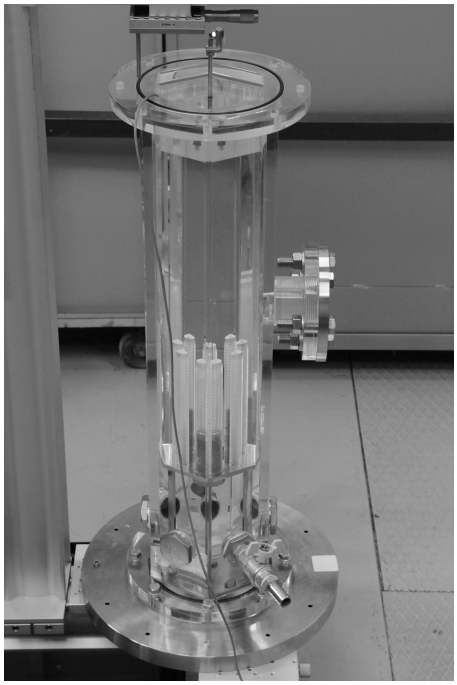

Fig. 6. Picture of the single enclosed hexagonal rod.

4.2 Added mass and damping with 3D effects flow: discussion of the experimental results

In Sargentini et al. [17], the free response of the twin-blades-supported enclosed prism is compared to the analytical solution. The 2D analytical model predicts a lower frequency and a higher damping ratio in water with respect to the measured one. In the next section we propose a correction factor basing on 3D flow considerations.

Free vibration response is measured both in air and in water, the results are listed in Tab. 1. Damping ratio in water is smaller with respect to air value. In fact, for narrow gaps, fluid inertia is very high and added mass is much higher than structural mass. As remarked by Daogang et al. [4], the damping ratio of the coupled system is proportional to the added damping and inversely proportional to the added mass. Hence, if gap is small enough (as in our case), the added mass effect is dominant on the added damping effect, and the resulting damping ratio in air is higher than in water.

Mulcahy [11] showed that the fluid damping force per unit length depends on the ratio between the internal cylindrical radius R_1 and its height H through the parameter χ:

$$\chi = 1 - \frac{R_1}{H} \tanh\left(\frac{H}{R_1}\right) \tag{7}$$

This means that, for slender structures ($H/R_1 \to \infty$), the damping force is due to the two-dimensional fluid flow around the 2D section, while, for stocky structures ($H/R_1 \to 0$), the damping force is due to the vertical fluid flow along the height of the vibrating cylinder due to the conditions of constant pressure at the top of the rod.

Our configuration is close to a stocky structure (H/R_1 roughly 8, and $\chi \approx 0$). This means that the damping force is

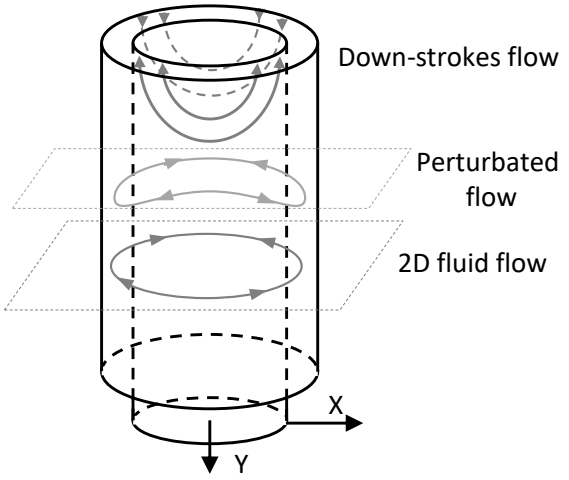

Fig. 7. Sketch of the flow features at the top of a rod oscillating along the x direction ($\theta = 0$) within a fluid-filled gap. This sketch applies both to cylinder and to hexagonal prisms.

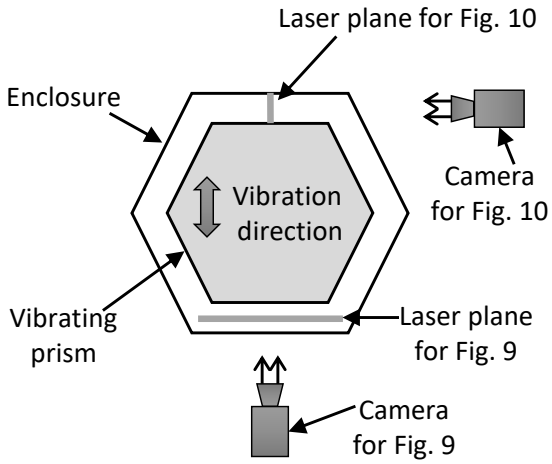

Fig. 8. Set-up of the PIV measurement system applied to the device of Fig. 6 (cross-section sketch). This system is used to record the velocity profiles of Fig. 9 and 10.

due to a 3D flow. Hence, it is unlikely to predict the damping by means of 2D coupled fluid-structure simulations. According to flow visualization made with PIV, near the top of the prism the fluid flow rises up to the free surface when the gap becomes larger than the initial condition and goes down to the gap when the gap becomes thinner [17]. The fluid behavior is symmetric with respect to the perpendicular line to the assembly displacement. This behavior depends on the pressure field. The vertical flow, referred to as down-strokes flow, damps down on a distance from the free surface of about the radius of the external cylinder R_2 (Fig.7).

The effect of this fluid movement is a loss of confinement and so, a loss of added fluid inertia. As a consequence, the added mass of the fluid M_{add} is lower than the theoretical value for a completely two-dimensional fluid-flow.

It is possible to apply a geometrical correction factor to the 2D pressure field in order to predict the frequency even in case of strong 3D effects.

This correction factor β only depends on the aspect ratio of the prism and it can be deduced from the ratio between the 2D fluid force $F_{f,2D}$ (given by equation 2) and the z-averaged fluid force calculated with a 3D pressure field $F_{f,3D}$ (given in [17]):

$$\beta = 2\frac{R_1 + b}{H} = \frac{F_{f,2D} - F_{f,3D}}{F_{f,2D}} \tag{8}$$

For the present experimental application $\beta = 0.3$. Sargentini et al. [17] found this correction factor effective to predict the frequency of the experimental device in water.

4.3 Fluid flow in the gap

The analytical solution of fluid flow given in the equation system 2 is now compared with the measured flow field within the experimental hexagonal assembly. As previously discussed in section 4.2, the solution for cylindrical structures can give a profitable description of flow within hexagonal gaps on some cases and zones.

Fig. 8 show the position of the PIV camera for the two subsequent figures. 2D planes are registered and used to extract velocity profiles at different heights.

In Fig. 9and in Fig. 10 we compare the experimental measured velocities across the gap and the analytical results of equations 9 and 10. A good agreement is shown far from the vertex of the hexagon, where vortex are present.

In Fig. 9 we show a velocity profile at mid-height of the prism. The profile is taken in the middle of the gap, along the hexagon's side. The measured vertical velocity w is almost zero, in agreement with the 2D hypothesis. The tangential velocity u is in good agreement with the cylindrical analytical solution far from the vertex of the hexagon, where vortex are present.

In Fig. 10 we show a velocity profile closer to the top of the prism. The profile is taken across the gap at mid-side of the hexagon. The measured vertical velocity w is high due to the 3D down-strokes flow. Nevertheless, the radial velocity v is still in good agreement with the cylindrical analytical solution.

5 Conclusion

In this paper we presented:

- a 2D analytical solution for forced vibration of a cylindrical enclosed rod with an narrow viscous gap. With respect to existing analytical formulations, the present one allows easier numerical calculation because of the absence of Bessel functions and it can be easily adapted to other geometries if the cross fluid section is equivalent.
- an energetic approach for defining the added mass and damping which is independent from geometry of the

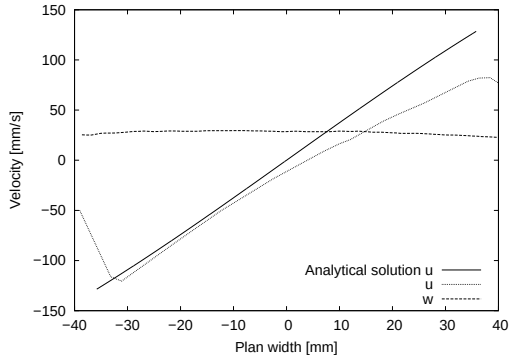

Fig. 9. Velocity profiles on the face of the prism compared to the analytical solution given by equations 9 at t=109 s and at mid-height of the prism.

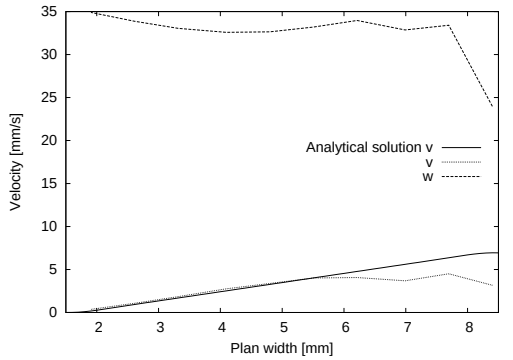

Fig. 10. Velocity profiles in the gap compared to the analytical solution given by equations 10 at t=120 s near the top of the prism. Cross-gap profile.

problem or if the solid is in forced or free vibrations.

- a comparison between the analytical solution, 2D numerical tool and experiments on the frequency and the damping ratio. Experimental observations of the flow within the liquid gap show that 3D flow is responsible for lower added mass effects in agreement with Mulchay's theory. This 3D fluid flow depends on the pressure field at the top of the prism (free surface). Taking into account 3D effects via the aspect ratio, as in equation 7, allows extending the 2D analytical solution to the 3D stocky structure.
- the comparison between the the measured flow velocity profiles for the hexagonal prism and the 2D cylindrical solutions. Radial and tangential velocities are in good agreement far from the corners.

6 Acknowledgments

This work has been supervised by Arnault Monavon, Jean-Paul Magnaud, Daniel Broc, whose contributions were essential.

References

[1] Paidoussis, M. P. (1998). Fluid-Structure Interactions: Slender Structures and Axial Flow. Accademic Press, San Diego, CA.

[2] Zhong, Y., Yang, X., Ding, D., Zou, Y., and Tsang, D. K. L. (2018). Numerical study of the dynamic characteristics of a single-layer graphite core in a thorium molten salt reactor. Nuclear Science and Techniques, 29:141. Doi: 10.1007/s41365-018-0488-8.

[3] Zhong, Y., Yang, X., Ding, D., Zou, Y., and Tsang, D. K. L (2018). Dynamic characteristics identification of two graphite bricks in molten salt reactor considering fluid-structure interaction Nuclear Engineering and Design, 335:409–416.

[4] Daogang, L., Aiguo, L., Chaohao, S., Junjie, D., Yang, H. and Qingyu, X. (2013). Experimental investigation on fluid-structure-coupled dynamic characteristics of the double fuel assemblies in a fast reactor. Nuclear Engineering and Design, 255:180–184.

[5] Wilson, D. E. (2011). Added mass and damping coefficients for hexagonal cylinder. Journal of fluids and structures, 5:503–519.

[6] Yang,C. -I., Moran, T. J. (1979). Finite-element solution of added mass and damping of oscillation rods in viscous fluids. Journal of applied mechanics, 46:519–523.

[7] Fujita, K. (1981). Vibrational characteristics and seimisc response analysis of colums group in liquid. Bulletin of JSME, 24:1994–2002.

[8] Chen, S. S. (1975). Vibration of nuclear fuel bundles. Nuclear Engineering and Design, 35:399-422.

[9] Chen, S. S., Wambsganss, M. W., Jendrzejczyk ,J. A. (1976). Added mass and damping of a vibrating rod in confined viscous fluids. Journal of Applied Mechanincs, 43(2):325–329.

[10] Fritz, R. J. (1972). The effect of liquids on the dynamic motions of immersed solids. Journal of Engineering for Industry, 94(1):167–173.

[11] Mulcahy, T. M. (1980). Fluid forces on rods vibrating in finite length annular regions. Journal of Applied Mechanics , 47:234–240.

[12] Fritz, R. J. (1976). Added mass and damping of a vibratory rod in confined viscous fluids (discussion). Journal of Applied Mechanincs, 43(4)699–700.

[13] Sargentini, L., Cariteau, B., Angelucci, M. (2014). Experimental and numerical analysis for fluid-structure interaction for an enclosed hexagonal assembly. ASME Pressure Vessels & Piping Conference, Anheim, USA. Paper PVP2014-28053.

[14] Chung, H., Chen, S. S. (1984). Hydrodynamic mass. Technical report CONF-840647–9, Argonne National Laboratory.

[15] Sargentini, L. (2014). Étude des mécanismes d'intéraction fluide-structure d'un cœur RNR-Na lors de l'évacuation d'une poche de gaz (in French).

PhD thesis, Pierre and Marie Curie University, Paris, France.

[16] Artini, G., Broc, D. (2017), Fluid structure interaction for tubes bundles: different homogenization methods. ASME Pressure Vessels & Piping Conference, Waikoloa, Hawaii (USA). Paper PVP2017-65727.

[17] Sargentini, L., Cariteau, B., Magnaud, J-P., Monavon, A., Artini, G. (2015). 3D effects in fluid flow during 2D vibrations: experimental analysis of FSI for an enclosed hexagonal assembly. ASME Pressure Vessels & Piping Conference, Boston, MA (USA). Paper PVP2015-45904.

[18] Deri, E. (2022). Some comments on added mass modeling for tube bundles under two-phase cross flow. Journal of Pressure Vessel Technology, 144:044503.

A Solution of the system of equation 2

The resulting velocity field if proportional to Stokes number and only depend on tangential coordinate: indeed, for small gap (high confinement) pressure doesn't vary radially. The following equations gives the dimensionless form of the developed azimuthal velocity, of the radial velocity and of the pressure:

$$\bar{u} = e^{i\bar{t}} \sin\bar{x} \left\{ -\frac{\eta \tanh(\frac{\sqrt{\sigma i}}{2}\bar{y})}{\tanh(\frac{\sqrt{\sigma i}}{2})} \frac{1-\tanh(\frac{\sqrt{\sigma i}}{2})}{1-\tanh(\frac{\sqrt{\sigma i}}{2}\bar{y})} + \left[\sqrt{\sigma i} + \eta\left(1 - \sqrt{\sigma i}\frac{1-\tanh(\frac{\sqrt{\sigma i}}{2})}{2\tanh(\frac{\sqrt{\sigma i}}{2})}\right)\right] \left(\frac{\cosh(\frac{\sqrt{\sigma i}}{2}\bar{y}) + \sinh(\frac{\sqrt{\sigma i}}{2}\bar{y})\tanh(\frac{\sqrt{\sigma i}}{2}) - 1}{2\tanh(\frac{\sqrt{\sigma i}}{2}) - \sqrt{\sigma i}}\right) \right\} \quad (9)$$

$$\bar{v} = e^{i\bar{t}} \cos\bar{x} \left\{ \left(\frac{\eta\sqrt{\sigma i}}{\tanh(\frac{\sqrt{\sigma i}}{2})} \frac{1-\tanh(\frac{\sqrt{\sigma i}}{2})}{1-\tanh(\frac{\sqrt{\sigma i}}{2}\bar{y})} + \frac{\bar{y}}{2}\frac{1-\tanh(\frac{\sqrt{\sigma i}}{2})}{\tanh(\frac{\sqrt{\sigma i}}{2})} \right) + \left[1 + \eta\left(\frac{1}{\sqrt{\sigma i}} - \frac{1-\tanh(\frac{\sqrt{\sigma i}}{2})}{2\tanh(\frac{\sqrt{\sigma i}}{2})}\right)\right] \left(\frac{\sinh(\frac{\sqrt{\sigma i}}{2}\bar{y})}{2\tanh(\frac{\sqrt{\sigma i}}{2}) - \sqrt{\sigma i}} + \frac{\cosh(\frac{\sqrt{\sigma i}}{2}\bar{y})\tanh(\frac{\sqrt{\sigma i}}{2}) - \tanh(\frac{\sqrt{\sigma i}}{2}) - \sqrt{\sigma i}\bar{y}}{2\tanh(\frac{\sqrt{\sigma i}}{2}) - \sqrt{\sigma i}} \right) \right\} \quad (10)$$

$$\bar{p} = \sigma i \cos\bar{x} e^{i\bar{t}} \frac{\tanh(\frac{\sqrt{\sigma i}}{2}) + \sqrt{\sigma i}}{2\tanh(\frac{\sqrt{\sigma i}}{2}) - \sqrt{\sigma i}} \quad (11)$$